International Journal of Automotive Technology, Vol. 24, No. 3, pp. 669–679 (2023)
DOI 10.1007/s12239–023–0056–z

pISSN 1229–9138/ eISSN 1976–3832

PARTICULATE MATTER CHEMICAL CHARACTERISTICS FROM A LIGHT-DUTY DIESEL ENGINE FUELED WITH PODE/DIESEL BLENDS

Xin Meng[1)*], Jing Tian[1)], Shuai Liu[2,3)], Ruina Li[2)], Jian Sun[1)] and Wenjun Liu[1)]

[1)]School of Mechanical and Electrical Engineering, Xuzhou University of Technology, Xuzhou 221018, China
[2)]School of Automotive and Traffic Engineering, Jiangsu University, Zhenjiang 212013, China
[3)]Tsinghua University Suzhou Automotive Research Institute, Tsinghua University, Suzhou 215200, China

(Received 11 January 2022; Revised 30 June 2022; Accepted 20 August 2022)

ABSTRACT–To evaluate the influence of polyoxymethylene dimethyl ethers (PODE) on particulate matter (PM) chemical features, PM samples emitted from diesel fuel and PODE/diesel blends at volume ratios of 10 %, 20 %, and 30 % (P10, P20, and P30) were characterized using gas chromatography-mass spectrometry, X-ray photoelectron spectroscopy (XPS), and Fourier transform infrared spectroscopic (FT-IR). Results showed that adding PODE in diesel fuel could increase the proportions of the lower carbon-atom-number components and the contents of oxygen-containing compounds in the soluble organic fractions extracted from PM samples. The ratio of oxygen to carbon (O/C), the functional groups, and the nanostructure of dry soot obtained from XPS showed that the O/C rose as the PODE volume ratio increased. The graphitization degree of dry soot decreased in the order: diesel fuel > P10 > P30 > P20. The relative content of hydroxyl functional groups exhibited the same trend, while the relative content of carbonyl functional groups exhibited an opposite trend with the graphitization degree. Moreover, according to FT-IR, both the branching degree and the relative content of hydrocarbon functional groups of aliphatics are influenced by the graphitization degree of dry soot. A turning point at P20 observed by analysis results above indicated that the chemical characteristics of PM could be affected not only by fuel properties but also by the process of fuel combustion and PM formation.

KEY WORDS : Diesel engine, Polyoxymethylene dimethyl ethers, Particulate matter, Soluble organic fractions, Surface functional groups

1. INTRODUCTION

Diesel engines are extensively applied in industry, modern farming, traffic, and freight transportation according to their higher thermal efficiency, economy, and durability (Roy *et al*., 2016). More than 90 % of particulate matter (PM) emitted from diesel engines is distributed at 10 nm ~ 1 μm of particle size, a kind of micro-nano scaled particle (Bagheri and Baar, 2018; Bermúdez *et al*., 2015). Also, diesel pm harms the atmospheric environment and mankind's health (Pirjola *et al*., 2017). The increasingly stringent emission legislations raise higher requirements for pm emissions of diesel engines. Besides, energy security issues are incredibly urgent all over the world, leading to the development of alternative fuels. Oxygenated fuels are considered to be promising alternative fuels, which play autonomous oxygen providing roles in the combustion and reduce pm emission of diesel engines (Zhang *et al*., 2020; Liu *et al*, 2019; Jamrozik *et al*., 2018).

**Corresponding author*. e-mail: mengxin@xzit.edu.cn

In recent years, oxygenated fuels such as methanol, ethanol, dimethyl carbonate (DMC), biodiesel, dimethyl ether (DME) have been extensively investigated as alternative fuels for diesel engines (Jamrozik *et al*., 2018; Alptekin, 2017; Suhaimi *et al*., 2018). Employing the oxygenated fuels above can promote the reduction of diesel PM, while there are some imperfections for their use. Compared with diesel fuel (DF), the lower boiling point and cetane number of methanol, ethanol, and DMC lead to air resistance and unstable combustion of diesel engines (Sun *et al*., 2013; Zhang, 2009; Sukjit *et al*., 2012). Biodiesel is perishable and corrosive (Weng *et al*., 2008). DME is gaseous at ambient temperature, and its greater vapor pressure and reduced viscosity, result in an alteration in the fuel feeding and the injection system of diesel engines (Wang *et al*., 2000). Polyoxymethylene dimethyl ethers (PODE) has a higher oxygen content and cetane number but a lower vapor pressure than DF, which is considered to be an ideal diesel additive (Burger *et al.*, 2010; Liu *et al*., 2016).

PODE is a kind of acetal polymer synthesized from methanol, Methylal, DME, trimeric formaldehyde, etc. with

the main chain of methoxy and the terminal group of methyl (Zhao *et al*., 2013; Ding *et al*., 2016; Zhang *et al*., 2015). There have been many investigations focused on the combustion and emissions of diesel engines fueled with the blended PODE fuels. Pellegrini *et al*. (2012, 2013, 2014) discussed the heat release rate and the emission performance in a single-cylinder diesel engine by blending PODE in DF at volume ratios of 7.5 %, 10 %, 12.5 %, 50 %, and neat PODE. Their studies confirmed that blending PODE in DF with volume ratios of 7.5 ~ 12.5 % presented a remarkable reduction in PM emission, while 50 % PODE showed a simultaneous optimization of PM and NO_x. Further, blends with high PODE volume ratios required a retuning of the injection system of the engine. Liu *et al*. (2015, 2017) indicated that blending PODE in DF at a volume ratio of 20 % resulted in earlier ignition, shorter ignition delay, and better in-cylinder combustion. In addition, the CO, HC, and PM emissions decreased with the PODE volume ratio increased from 10 to 30 %. Zhang *et al*. (2016) analyzed the particle size distributions and the number concentrations of PM emitted from a turbocharged diesel engine fueled with DF, 10 ~ 30 % blended PODE, and 100 % PODE. Their results showed that the particle size distributions of DF and blended PODE was ranged from 10 to 200 nm, while PM of PODE was nuclei mode with a range of no more than 30 nm. As the PODE volume ratio increased, the emission of small-size PM increased, while that of large-size PM decreased. Liu *et al*. (2021) compared the particle microscopic morphology by DF and blended PODE respectively. Blending PODE in DF resulted in smaller microscopic morphology of particles and an increase of the agglomeration degree between particles. The changes in PM morphological characteristics depends on the effect of PODE on the chemical reaction path, the intermediate species, and the PM formation process in the combustion process. Tan *et al*. (2018) analyzed the influencing factors of dry soot (DS) reduction by PODE in a diffusion flame. The results showed that adding PODE could dilute the aromatics and enhance the oxygen content of DF, which is beneficial to DS reduction. OH^* and CH_3O^* radicals play a DS suppression role in the combustion. According to Ren *et al*. (2019), an n-heptane/PODE chemical kinetic mechanism was put forward for ignition and DS generation prediction. Their study indicated that the lack of C-C bond in the PODE molecules lessened the generation of DS.

As discussed above, previous studies focused on the effect of PODE on the combustion performance of diesel engines and PM emissions. Nevertheless, detailed information on the chemical features of PM by PODE/diesel blends is rarely investigated. That is to say, the particle structure characteristics, the surface functional groups, and the soluble organic fraction (SOF) in PM are not well understood to date. In our previous study (Meng *et al.*, 2019), we found that the decomposition reactions of PODE will accelerate the formation of the CH_2O^* and OH^* radical pool fueled with blended PODE. In addition, we also found that blending PODE in DF is beneficial to increasing the oxidation activity of PM (Tian *et al*., 2019). Therefore, in order to explore the relationship between PODE decomposition reaction and PM oxidation activity, it is necessary to carry out the research on the chemical features of PM by PODE/diesel blends.

In this study, PODE was mixed with DF at volume ratios of 0 ~ 30 %. PM samples were sampled from a YD480Q diesel engine and pretreated to investigate the PM chemical characteristics. Gas chromatography-mass spectrometry (GC-MS), X-ray photoelectron spectroscopy (XPS), and Fourier transform infrared spectroscopic (FT-IR) were employed to explore impacts of PODE on the soluble organic fractions (SOF) components in PM and surface functional groups of DS, respectively.

2. EXPERIMENTAL DEVICE AND METHODS

2.1. Test Fuels

In this study, the effects of blending PODE in commercial 0# DF on the chemical characteristics of PM were investigated. DF with a sulfur content of less than 0.001 % was produced by PetroChina. PODE was provided by Heze Chenxin Company. PODE is a kind of acetal polymer with the molecule formula of $CH_3O(CH_2O)_nCH_3$, where n represents the polymerization degree and $n \geq 2$ (Burger *et al*., 2010). The mass fractions of $PODE_3$, $PODE_4$, $PODE_5$, and $PODE_6$ (3, 4, 5, and 6 stand for the polymerization degree of $–CH_2O$) are 45.67 %, 29.39 %, 17.39 %, and 7.10 %, respectively. Table 1 summarizes the properties of DF and PODE (Liu *et al*., 2016). Compared with DF, high oxygen content and higher cetane number of PODE are beneficial to improve the localized hypoxia during the in-cylinder combustion, nevertheless, the lower low heating value and kinematic viscosity decrease the power performance of diesel engines (Liu *et al*., 2017). Blended PODE with volume ratios of 0 %, 10 %, 20 %, and 30 % were recorded as DF, P10, P20, and P30, respectively.

2.2. Experimental Devices and PM Sampling

The schematic for PM sampling and analysis instruments are shown in Figure 1. PM samples were collected from a YD480Q direct injection light-duty diesel engine, and the main specifications of the test engine were shown in our previous work (Tian *et al*., 2019). In this study, the working condition of the test engine was kept at 2500 r/min of speed and 69 N·m of torque, respectively. The PM sampling system involved a PM sampler, a sampling filter, as well as a vacuum pump. To complete the chemical analyses, the quartz fiber filters with a diameter of 47 mm and the heat-resistance of 900 °C by Whatman (Maidstone, UK) were adopted. The filters were pretreated at 600 °C for 2 hours to eliminate the effects of pollutants, according to

Table 1. Properties of DF and PODE.

Fuel	Density ($g \cdot cm^{-3}$)	w(O) (%)	w(C) (%)	w(H) (%)	Cetane number	Low heating value ($MJ \cdot kg^{-1}$)	Kinematic viscosity ($mm^2 \cdot s^{-1}$)
DF	0.84	0	87.4	12.6	51	42.6	3.05
$PODE_3$	1.02	47.1	44.1	8.8	78	19.1	1.05
$PODE_4$	1.06	48.2	43.4	8.4	90	18.4	1.75
$PODE_5$	1.1	49.0	42.9	8.1	100	17.8	2.24
$PODE_6$	1.13	49.6	42.5	7.9	104	17	--
PODE	1.051	47.9	43.5	8.5	≥70	18.6	1.40

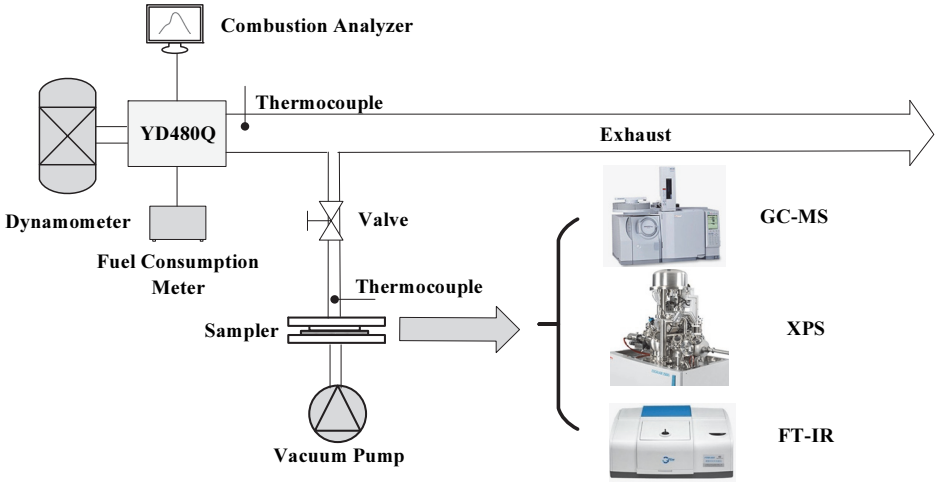

Figure 1. Schematic for PM sampling and analysis instruments.

Wang *et al*. (2020). After replacing with a new fuel, the engine was operated for no less than 30 min to ensure the previous fuel was purged with the valve closed. Then, opened the valve to sample PM for 30 min at a sampling temperature of 52 ± 2 °C by 24 L/min of flow.

2.3. Analytical Technology

2.3.1. GC-MS

PM consists of dry soot (DS), SOF, mineral salt and ash. SOF attaches to DS surface. Gas chromatography-mass spectrometry (Clarus SQ8, PerkinElmer, USA) was applied to observe the components of SOF in PM samples produced from various PODE/diesel blends. The SOF was extracted by Soxhlet extraction for 24 hours in dichloromethane (DCM) and then concentrated the solution to 1 mL, according to Shah *et al*. (2012). As suggested by Shi *et al*. (2019), a chromatographic column (30 m × 250 μm) was used for GC, while the column temperature was raised from 50 °C up to 300 °C at a heating rate of 10 °C/min, and then maintained at 300 °C for about 10 min. High-purity helium gas with a concentration of 99.999 % was adopted as the carrier gas, and the current speed is 20 mL/min. For MS, the ion source was electron impact at 280 °C.

2.3.2. XPS

X-ray photoelectron spectroscopy (ESCALAB 250Xi, Thermo Scientific, USA) was used to identify the chemical states, the ratio of O/C, as well as the surface functional groups of DS. The DS was ultrasonically extracted in DCM and then separated by centrifugation, as introduced by Wang *et al*. (2013). The DS samples were analyzed via the survey scan and the narrow scan (C1s spectra). For the survey scan, the energy range was 0 ~ 1000 eV with a step of 1 eV, and the pass energy was 100 eV. For C1s spectra, the energy range was 278 ~ 298 eV with a step of 0.1 eV, and the pass energy was 20 eV. The C1s spectra was curve-fitted by using XPSPeak software.

2.3.3. FTIR

Fourier transform infrared spectroscopic with a resolution of 0.1 cm^{-1} (Nicolet iS5, Thermo Scientific, U.S.) was adopted to investigate the surface functional groups of DS. DS samples were pretreated according to Section 2.3.2, and then mixed with potassium bromide (KBr) and scanned at the middle infrared spectrum with a spectral region of 400 ~ 4000 cm^{-1} to acquire the infrared spectrums. The pure KBr sample was examined to correct the background. As suggested by Ibarra *et al*. (1996), Pan *et al*. (2022) and Yu

et al. (2016), the Gaussian curve-fitting method was adopted to obtain the relative content of the aliphatic hydrocarbons.

3. RESULTS AND DISCUSSION

3.1. Engine Performance and Fuel Economy

Figure 2 displays the in-cylinder pressure fueled with the PODE/diesel blends at 2500 r/min and 69 N·m. As shown in Figure 2, the maximum combustion pressure becomes larger with the peak phase advanced as the PODE volume ratio increases. This is because the high volatility and the high oxygen content of PODE increase the mixing rate and the chemical reaction rate of the blended fuels (Kalghatgi *et al*., 2007). Furthermore, the higher cetane number of PODE shortens the ignition delay and advances the ignition timing which leads to a better constant-volume combustion (Liu *et al*., 2016). It was consistent with Burger *et al*. (2010), Gao *et al*. (2019), Iannuzzi *et al*. (2017), Liu *et al*. (2015) and Pellegrini *et al*. (2012) results.

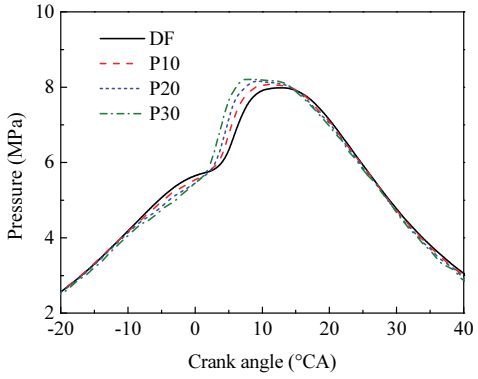

Figure 2. In-cylinder pressure fueled with the PODE/diesel blends.

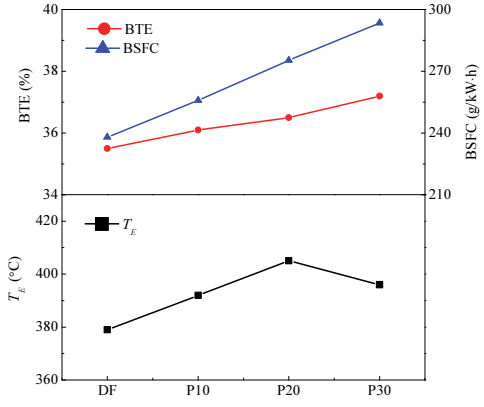

Figure 3. BTE, BTFC and T_E fueled with the PODE/diesel blends.

The brake thermal efficiency (BTE), brake specific fuel consumption (BTFC) and exhaust temperature (T_E) are illustrated in Figure 3. BTE and BTFC become larger by blending PODE in diesel. Lower low heating value of PODE causes a drop of the engine power, leading to a higher fuel consumption per cycle to achieve the same output power of DF (Pellegrini *et al*., 2012). Therefore, BTFC tended to increase as the PODE blending ratio increases. Blending PODE increases the BTE is mainly due to the lower viscosity, higher oxygen content, and higher cetane number of PODE. Blending PODE in DF results in better atomization, ignition, and combustion (Liu *et al*., 2016). From the T_E curve, the T_E of DF, P10, P20 and P30 are 379 °C, 392 °C, 405 °C and 396 °C respectively. T_E climbs to its peak at P20 and decreases at P30. T_E climbs is because PODE improves combustion characteristics. However, the higher evaporation heat absorption of PODE causes a lower in-cylinder temperature before combustion. Shorter ignition delay is unfavorable to fuel atomization and diffusion, and leads to an insufficient local combustion with the fuel consumption rises. In addition, in our previous study (Meng *et al*., 2019), the peak of apparent heat release rate decreased while PODE blending ratio is increased resulting from the lower low heating value of PODE. It brings a drop of in-cylinder temperature at P30. It is similar with Xie *et al*. (2017) result. They found that the in-cylinder temperature dropped with the PODE blending ratio was no less than 30 %.

The effects of PODE on combustion characteristics for diesel engines have been investigated in several studies and they got similar results. In this study, we focus on the chemical features of PM fueled with the PODE/diesel blends and address Section 3.2 to 3.4 as our main content.

3.2. SOF Components in PM

The example of the total ion chromatogram of SOF in PM is shown in Figure 4. SOF components, extracted from PM samples fueled with DF, P10, P20, and P30, show a retention time of 10 ~ 30 min. The total ion chromatograms of various SOF samples present a characteristic bulge peak with the retention time of 19.2 min, 18.8 min, 18.6 min, and 18.8 min, respectively, as the PODE volume ratio increases. A substance with a lower number of carbon atoms flows out of the chromatographic column earlier than a substance with a higher number of carbon atoms (Zhou, 2017). It indicates that compared with DF, blended PODE is conducive to improving the combustion, and promoting the oxidation of components with high-carbon-atom-number to components with low-carbon-atom-number. Furthermore, the absence of the C-C bond in the PODE molecule plays a passive role in the formation of soot precursors. Referring to the spectrum library, the main SOF components are determined. The percentages of the SOF components are obtained by the peak-area normalization. Table 2 lists the main SOF components in PM fueled with the PODE/diesel

Table 2. Main SOF components in PM fueled with the PODE/diesel blends.

No.	Name	Molecular formula	Mass fraction (%) / Test fuel			
			DF	P10	P20	P30
1	Mexadecane	$C_{16}H_{34}$	4.01	5.48	5.38	5.75
2	1-decanol, 2-hexyl-	$C_{16}H_{34}O$	1.68	2.43	3.46	2.47
3	Dibutyl phthalate	$C_{16}H_{22}O_4$	1.10			
4	Pentadecane,2,6,10-trimethyl-	$C_{18}H_{38}$	1.88			
5	Phthalic acid, isobutyl 2-methylpent-3-yl ester	$C_{18}H_{26}O_4$		1.55		2.79
6	Eicosane	$C_{20}H_{42}$	3.05	6.24	6.12	6.77
7	Heneicosane	$C_{21}H_{44}$	8.50	7.62	6.29	6.33
8	Carbonic acid, octadecyl vinyl ester	$C_{21}H_{40}O_3$	4.11	4.46	6.06	4.38
9	1-propyl 9-octadecenoate	$C_{21}H_{40}O_2$			1.68	
10	Carbonic acid, decyl undecyl ester	$C_{22}H_{44}O_3$		1.69	1.08	
11	Octadecane,2,6,10,14-tetramethyl	$C_{22}H_{46}$		1.50	1.30	1.38
12	Nonadecane, 2, 6, 10, 14-tetramethyl-	$C_{23}H_{48}$				1.12
13	11-methyltricosane	$C_{24}H_{50}$	5.52	4.52	3.87	3.41
14	Pentacosane	$C_{25}H_{52}$	8.80	5.98	5.46	6.14
15	2-methylhexacosane	$C_{27}H_{56}$	1.32	1.05		
16	Heptacosane	$C_{27}H_{56}$	1.20			
17	Didecyl phthalate	$C_{28}H_{46}O_4$			1.06	
18	Hentriacontane	$C_{31}H_{64}$	6.54	2.75	1.99	2.22

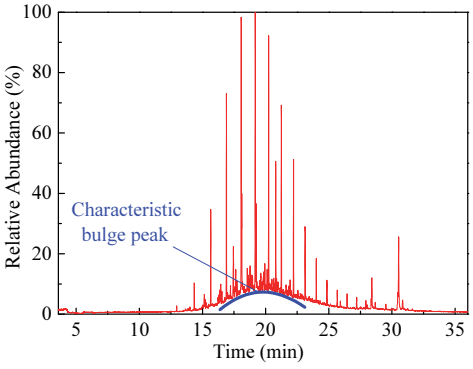

Figure 4. Example of the total ion chromatogram of SOF in PM.

blends with percentages of no less than 1 %. SOF extracted from PM samples is composed of not only n-alkanes and branched alkanes, but also alcohols and organic acid esters as well. N-alkanes and branched alkanes mainly evaporated or cracked by diesel. Alcohols and organic acid esters are the combustion products containing oxygen.

To study the effect of PODE on carbon chains, components of SOF listed in Table 2 are counted by carbon-atom-number in the molecular formula and compared in Figure 5. Blending PODE in DF is beneficial to increase the proportion of low-carbon-atom-number components and decrease the proportion of high-carbon-atom-number components. The carbon-atom-number of the components in various SOF samples is mainly distributed in C16-C31. The proportions of the components with a lower carbon-atom-number (C16-C22) are 24.33 %, 30.97 %, 31.37 %, and 29.85 %, respectively, fueled with DF, P10, P20, and P30. While the proportions of the components with a higher carbon-atom-number (C23-C31) are 23.38 %, 14.30 %, 12.38 %, and 12.89 %, respectively. The proportions of C16-C22 increase first and then decrease as the PODE volume fraction is 30 %. However, the proportions of C23-C31 show an opposite trend. High cetane number of PODE and oxygen in PODE molecule promote the in-cylinder combustion. Combustion temperature rises and more oxygen is involved in the reactions. It promotes the oxidation of high-carbon-atom-number components to low-carbon-atom-number components. However, blending PODE in DF promotes an increase in fuel consumption, a decrease in power performance, a shorter ignition delay, and insufficient local combustion. It leads to a lower in-cylinder temperature of P30 compared to P20 and is detrimental to the oxidation of high-carbon-atom-number components to low-carbon- atom-number components.

Figure 6 displays the proportions of various SOF components in PM fueled with the PODE/diesel blended fuels. The content of n-alkanes in SOF is more than that of the other SOF components. The contents of hydrocarbons (n-alkanes and branched alkanes) decrease, while oxygen-containing components (alcohols and organic acid esters) increase by blending PODE in DF. The proportions of n-alkanes, branched alkanes, alcohols, and organic acid esters are 32.10 %, 8.73 %, 1.68 %, and 5.21 %, respectively, fueled with DF. Compared to DF, the proportion of n-alkanes decreases 3.02 %, 6.86 %, and

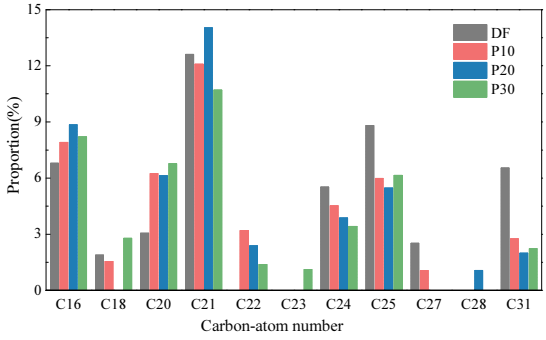

Figure 5. Distributions of components with various carbon-atom-number in SOF.

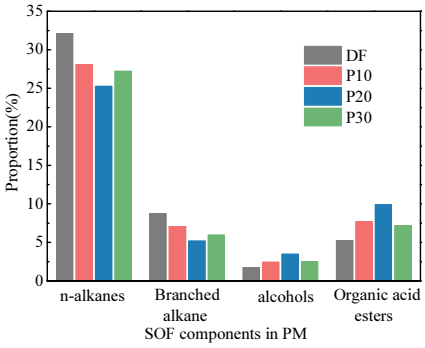

Figure 6. Proportions of SOF components in PM.

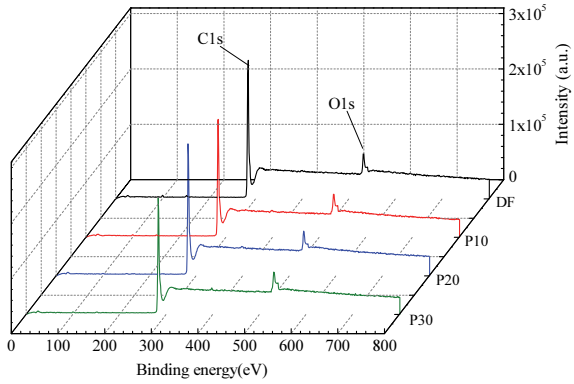

Figure 7. XPS survey scan spectra of the DS samples fueled with the PODE/diesel blends.

Table 3. Relative contents of C and O and the ratios of O/C for the DS samples.

Items	DF	P10	P20	P30
C Relative content (%)	86.27	86.13	85.79	85.55
O Relative content (%)	13.73	13.87	14.21	14.45
O/C	0.159	0.161	0.166	0.169

4.89 %; the proportion of branched alkanes decreases 1.67 %, 3.56 %, and 2.81 %; the proportion of alcohols increases 0.75 %, 1.78 %, and 0.79 %; the proportion of organic acid esters increases 2.49 %, 4.67 %, and 1.96 %, respectively, as the PODE volume fraction is from 10 to 30 %.

The formation of PM can be divided into four stages: the formation of linear hydrocarbonds (C_2H_2, C_2H_x, C_3H_x, C_4H_x, etc) in DF decomposition, the formation of soot precursors and carbon nuclei, particle growth by collision and condensation, and particle oxidation (Cao *et al*., 2020). The decomposition of PODE was described by Tan *et al*. (2018) as shown in the Equation (1). The main products of PODE decomposition are methoxy radical (CH_3O^*), methyl radical (CH_3^*), and formaldehyde (CH_2O).

$$CH_3O(CH_2O)_nCH_3 \rightarrow CH_3O^* + CH_3^* + n\ CH_2O \quad (1)$$

Oxygen in CH_3O^* can be converted to produce oxidising species (O^*, HO^*, HO_2^*, H^*) through thermal decomposition or react with molecular oxygen. According to Bui *et al*. (2020), hydrocarbonds plus HO^* goes to hydroxy compounds (R-OH, where R is alkyl) and H^*, while C_mH_nO plus H^* produces hydrocarbonds and carbonyl compounds (R-C=O), where m and n are the numbers of carbon atoms and oxygen atoms respectively. Furthermore, the formation of oxidising species promotes the consumption of hydrocarbons. Blengding PODE in diesel produces more oxidising species which are instrumental in producing R-OH (alcohols) and R-C=O (organic acid esters). More alcohols and organic acid esters adhere on the surface of the PM. Therefore, the proportions of alcohols and organic acid esters in SOF increase. However, the in-cylinder temperature drops as PODE blending ratio is 30 % and the thermal decomposition of PODE and CH_3O^* is suppressed. The content of oxidising species decreases. It suppresses the generation of R-OH (alcohols) and R-C=O (organic acid esters). Therefore, the proportions of alcohols and organic acid esters in SOF drops at P30.

3.3. Surface Functional Groups by XPS

XPS analysis provides the information of elements, functional groups, and nanostructure in the surface of DS samples. Figure 7 shows the XPS survey scan spectra of the DS samples fueled with the PODE/diesel blends. Every DS sample presents two prominent peaks: carbon (C1s) at a binding energy of 284 eV and oxygen (O1s) at 531 eV. The relative contents of C and O and the ratios of O/C for various DS samples are listed in Table 3. The O/C, calculated by contrasting the areas of C1s and O1s peaks, is 0.159 for the DS sample by DF, and 0.002, 0.007, and

Table 4. Assignments of various functional groups for C1s spectra (Mustafi *et al*., 2010; Smith *et al*., 2016).

Binding energy (eV)	Functional group	Assignment
283.6	C-C	Cyclopentane ring atoms or fullerene
283.9 ~ 285.1	sp2	sp2 bonded carbon
284.5 ~ 285.3	sp3	sp3 bonded carbon
285.9	C-OH	Ether and hydroxyl bonded C
286.7 ~ 288.36	C=O	Carbonyl groups
289.2 ~ 290.44	COO	Carboxyl, lactone and ester groups
291.0	π-π*	Shake-up satellite peak due to π-π* transitions in aromatic rings

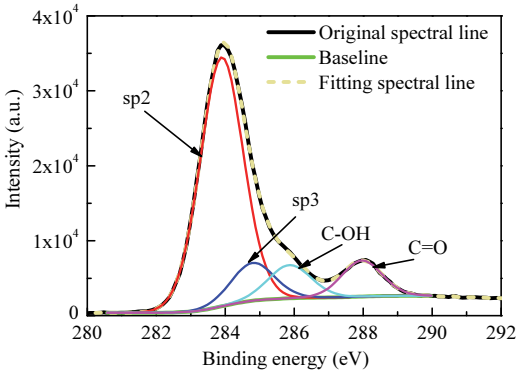

Figure 8. Example of curve-fitted C1s spectra for DS.

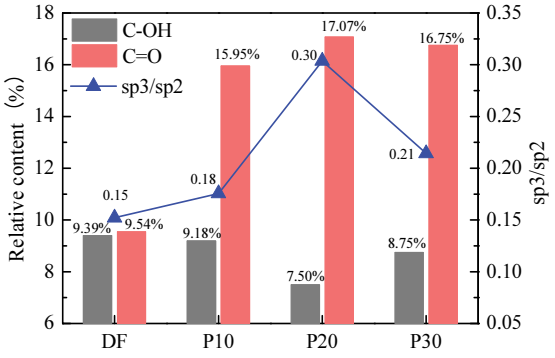

Figure 9. Relative content of C-OH and C=O and sp3/sp2 of C1s spectra.

0.010 higher for the DS samples by P10, P20, and P30 blended fuels respectively. With the adjunction of PODE, the rise of the oxygen content in the blended fuels results in an improvement of the relative content of O atoms.

To investigate the functional groups and the nanostructure in the surface of DS samples, C1s spectra for DS samples fueled with the PODE/diesel blends are curve-fitted for individual elements using Gaussian/Lorentzian line shapes, according to Mustafi *et al*. (2010, 2016). Assignments of various functional groups for C1s spectra are listed in Table 4. Oxygen functional groups and their relative contents can be identified by the relative peak position and the areas of the corresponding peaks. The example of curve-fitted C1s spectra for DS is displayed in Figure 8. According to the assignments in Table 4, C1s spectra were deconvoluted into four peaks. The carbon bonding state is differentiated based on hybridization: sp2 at 283.9 eV and sp3 at 284.8 eV, where sp2 characterizes the lattice structure of carbon and sp3 depicts the amorphous form of carbon (Savic *et al*., 2016). The oxygen functional groups are classified into two categories: hydroxyl (C-OH) functional groups at 285.9 eV and carbonyl (C=O) functional groups at 288.0 eV. The relative contents of C-OH and C=O and the ratio of sp3/sp2 are shown in Figure 9.

The ratio of sp3/sp2 is used to describe the nanostructure of DS. The higher value of sp3/sp2, the less graphitization (ordered structure) degree of DS (Wang *et al*., 2020). The value of sp3/sp2 increases then decreases with PODE volume fraction increases and climbs to the peak at P20, indicating a more disordered structure of the P20 DS sample. Blending PODE in DF leads to a higher net production of OH^* radicals as mentioned earlier. Due to a better reactivity between OH^* radicals and carbon atoms in edge site positions of the carbon layer, the graphitization degree of DS decreases (Tan *et al*., 2018). However, compared with P20, a lower incylinder temperature of burning P30 inhibits the formation of OH^* radicals, leading to a more graphitization degree of the P30 DS sample than P20 DS. The lower graphitization degree of DS indicates the more irregular sections of the lattice structure, which provides more chemically active sites for oxygen-containing groups in the environment. Therefore, the oxygen functional groups are easier to form on the surface of the primary carbon particles. Meanwhile, blending PODE in DF can improve combustion, where the higher combustion temperature can promote the oxidation of oxygen-containing functional groups in DS. As well as, the bond energy of C-O is lower than that of C=O. Affected by the factors above, the relative content of C=O has the same trend as sp3/sp2, while the relative content of C-OH has an opposite direction.

3.4. Surface Functional Groups by FT-IR

To further explore the influence of PODE on the surface functional groups of DS, FT-IR spectra of the DS samples fueled with various PODE/diesel blends are curve-fitted and semi-quantitatively analyzed. Table 5 lists the typical FT-IT peaks observed for surface functional groups of DS (Ibarra *et al*., 1996; Cain *et al*., 2010; Weng, 2010). Figure 10 shows the FT-IR spectra of studied DS samples. As shown in Figure 10, all FT-TR spectra show adsorption band diagrams with similar peak positions, which indicates that the composition of functional groups in soot particles is similar. The main functional groups of DS samples include hydroxyl (–OH) in the 3000 ~ 3693 cm^{-1} site, aromatics (C-H) and aliphatic hydrogen (–CH_2 and –CH_3) in the 2650 ~ 3000 cm^{-1} site, and the oxygen functional groups (C-O, C=O, and -OH), C-O-R structures, and aromatic rings (C=C) in the 830 ~ 1800 cm^{-1} site. As proposed by Shi *et al*. (2019), the infrared absorption peak of inorganic salts belonging to the 400 ~ 800 cm^{-1} zone is probably influenced by the quartz fiber filters.

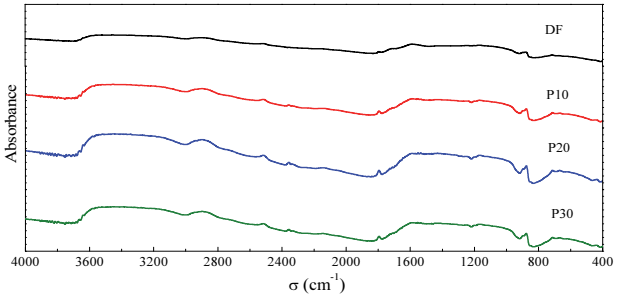

Figure 10. FT-IR spectra of the DS samples fueled with the PODE/diesel blends.

Figure 11 shows the example of curve-fitted FT-IR spectra for the DS. Asymmetric vibration of –CH_3 is observed at 2954 cm^{-1} and 2914 cm^{-1}. While asymmetric vibration of -CH_2, as well as stretching vibration of -CH_2 in aliphatics are observed at 2862 cm^{-1} and 2738 cm^{-1} separately. The contrast of the intensities of the peaks above shows that the intensity of asymmetric vibration is greater than stretching vibration, indicating the aliphatic functional groups in DS mainly exist in the form of short-chain alkyl functional groups (Yu *et al*., 2016). The 2862 to 2738 cm^{-1} peak area ratio (A_{2862}/A_{2738}) can be used to characterize the branching degree of aliphatics in DS (Ibarra *et al*., 1996). Moreover, stretching vibration of C=C in phenolic aromatic rings is observed at 1595 cm^{-1}, and the 2862 to 1595 cm^{-1} peak area ratio (A_{2862}/A_{1595}) can be adopted to characterize the relative content of hydrocarbon functional groups in aliphatic (Ibarra *et al*., 1996).

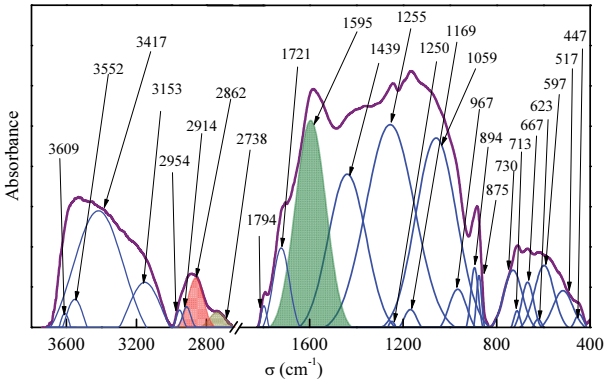

Figure 11. Example of curve-fitted FT-IR spectra for the DS.

Table 5. Typical FT-IT peaks observed for surface functional groups of DS.

Peak position (cm^{-1})	Functional group	Vibration mode
3100 ~ 3560	-OH	Stretching vibration
3030 ~ 3060	C-H	Stretching vibration of C-H in aromatics
2910 ~ 2975	-CH_3	Asymmetric vibration of -CH_3 in naphthenes or aliphatics
2860 ~ 2905	-CH_2	Asymmetric vibration of -CH_2 in naphthenes or aliphatics
2700 ~ 2870	-CH_2	Stretching vibration of -CH_2
1765 ~ 1800	C=O	Stretching vibration of C=O in aromatic esters and anhydrides
1720 ~ 1750	C=O	Stretching vibration of C=O in aliphatics
1690 ~ 1720	C=O	Stretching vibration of C=O in aldehydes, ketones, and acids
1630 ~ 1650	C-O-R	Stretching vibration of aliphatic amides
1595 ~ 1620	C=C	Stretching vibration of C=C in phenolic aromatic rings or fused rings
1560 ~ 1590	-COO	Asymmetric vibration of -COO in carboxylic acids
1490 ~ 1536	C=C	Stretching vibration of C=C in aromatic rings
1435 ~ 1460	-CH_3	Asymmetric deformation vibration of -CH_3
1375 ~ 1400	-CH_3	Stretching vibration of -CH_3
1030 ~ 1345	-C-O	Stretching vibration of -C-O in phenols, ethers, alcohols, esters
915 ~ 979	-OH	Out-plane vibration of -OH isolated in benzene rings
700 ~ 867	C-H	Out-plane vibration of C-H in aromatics

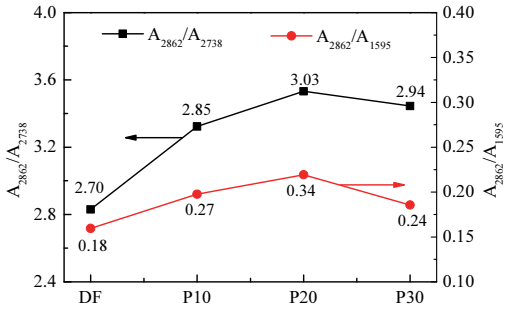

Figure 12. A_{2862}/A_{2738} and A_{2862}/A_{1595} for the DS samples fueled with the PODE/diesel blends.

A_{2862}/A_{2738} and A_{2862}/A_{1595} for the DS samples fueled with the PODE/diesel blends are shown in Figure 12. Both A_{2862}/A_{2738} and A_{2862}/A_{1595} rise as the PODE volume ratio goes up, and climb to the peak at P20. It indicates that blending PODE in DF is instrumental in improving the branching degree and the relative content of hydrocarbon functional groups of aliphatics. Qu (2017) observed the fracture layer of the lattice structure in DS increased with the decrease of the graphitization degree, which promoted the combination of hydrocarbon functional groups in the lattice structure. XPS test indicates that the DS sample fueled with P20 presents a lower graphitization degree than the other DS samples, consistent with the result of A_{2862}/A_{1595}.

4. CONCLUSION

In this research, the chemical characteristics of PM emitted from a light-duty diesel engine by the PODE/diesel blends were evaluated by analytical techniques of GC-MS, XPS, and FT-IR. The influence of PODE volume fraction on SOF components in PM and nanostructure and surface functional groups of DS were investigated. The following points are the main conclusions of this work.

(1) PODE plays a more active role in raising the proportions of the components with a lower carbon-atom-number (C16-C22) and reducing that of the components with a higher carbon-atom-number (C23-C31) for its inhibition of soot precursor formation and improvement of combustion. The contents of oxygen-containing components increase, and the contents of hydrocarbons decrease according to the high oxygen content of PODE.

(2) The addition of PODE in DF improves the O/C ratio of DS and decreases the graphitization degree. The contents of C=O and C-OH functional groups can be affected by the graphitization degree of DS and the combustion environment. Blending PODE in DF is conducive to increasing the content of C=O and decreasing that of C-OH.

(3) The surface functional groups of DS are composed of hydroxyls, aromatics, aliphatics, and oxygen functional groups. The relative content of hydrocarbon functional groups and the branching degree of aliphatics are influenced by the graphitization degree of DS. A higher branching degree and the relative content of hydrocarbon functional groups in aliphatics can be obtained by adding PODE in DF.

The analysis results in this work show a turning point as the PODE volume fraction is more than 20 %. It indicates that the PM chemical characteristics can be influenced by the fuel characteristics, the in-cylinder combustion process, the formation process of primary carbon particles, as well as the growth process of the particle surface.

ACKNOWLEDGEMENT–This work was financially supported by doctor of entrepreneurship and innovation in Jiangsu Province (JSSCBS20211280), Natural Science Research of Jiangsu Higher Education Institutions of China (18KJB470006), Six Talent Peaks Project in Jiangsu Province (GDZB-128), Zhenjiang Key R&D Program-Social Development (SH2020006), and the Science Research Project of Xuzhou University of Technology (XKY2019217).

REFERENCES

Alptekin, E. (2017). Evaluation of ethanol and isopropanol as additives with diesel fuel in a CRDI diesel engine. *Fuel*, **205**, 161–172.

Bagheri, M. and Baar, R. (2018). Simultaneous application of exhaust gas recirculation and non-constant injection rates to reduce NOx and soot emissions in diesel engines. *Emission Control Science and Technology* **4**, **1**, 4–14.

Bermudez, V., Luján, J. M., Ruiz, S., Campos, D. and Linares, W. G. (2015). New European Driving Cycle assessment by means of particle size distributions in a light-duty diesel engine fuelled with different fuel formulations. *Fuel*, **140**, 649–659.

Bui, T. T., Balasubramanian, D., Hoang, A. T., Konur, O., Nguyen, D. C. and Tran, V. N. (2021). Characteristics of PM and soot emissions of internal combustion engines running on biomass-derived DMF biofuel: A review. *Energy Sources, Part A: Recovery, Utilization, and Environmental Effects*, 1–22.

Burger, J., Siegert, M., Ströfer, E. and Hasse, H. (2010). Poly (oxymethylene) dimethyl ethers as components of tailored diesel fuel: Properties, synthesis and purification concepts. *Fuel* **89**, **11**, 3315–3319.

Cain, J. P., Gassman, P. L., Wang, H. and Laskin, A. (2010). Micro-FTIR study of soot chemical composition—evidence of aliphatic hydrocarbons on nascent soot surfaces. *Physical Chemistry Chemical Physics* **12**, **20**, 5206–5218.

Cao, D. N., Hoang, A. T., Luu, H. Q., Bui, V. G. and Tran, T. T. H. (2020). Effects of injection pressure on the NOx and PM emission control of diesel engine: A review under the aspect of PCCI combustion condition. *Energy*

Sources, Part A: Recovery, Utilization, and Environmental Effects, 1–18.

Ding, T., Shen, Z. and Zhang, J. (2016). Research progress on synthesis and application of polyoxymethylene dimethyl ethers. *Chemical Industry and Engineering Progress* **35**, **3**, 758–765.

Gao, W., Liu, J., Sun, P., Yang, C. and Fang, J. (2019). Gaseous emissions and particle microstructure characteristics of PODE/diesel blend fuel. *Int. J. Automotive Technology* **20**, **3**, 607–617.

Iannuzzi, S. E., Barro, C., Boulouchos, K. and Burger, J. (2017). POMDME-diesel blends: Evaluation of performance and exhaust emissions in a single cylinder heavy-duty diesel engine. *Fuel*, **203**, 57–67.

Ibarra, J., Munoz, E. and Moliner, R. (1996). FTIR study of the evolution of coal structure during the coalification process. *Organic Geochemistry* **24**, **6-7**, 725–735.

Jamrozik, A., Tutak, W., Pyrc, M., Gruca, M. and Kočiško, M. (2018). Study on co-combustion of diesel fuel with oxygenated alcohols in a compression ignition dual-fuel engine. *Fuel*, **221**, 329–345.

Kalghatgi, G. T., Risberg, P. and Ångström, H. (2007). Partially pre-mixed auto-ignition of gasoline to attain low smoke and low NOx at high load in a compression ignition engine and comparison with a diesel fuel. *SAE Paper No*. 2007-01-10006.

Liu, H., Wang, Z., Wang, J., He, X., Zheng, Y., Tang, Q. and Wang, J. (2015). Performance, combustion and emission characteristics of a diesel engine fueled with polyoxymethylene dimethyl ethers (PODE3-4)/diesel blends. *Energy*, **88**, 793–800.

Liu, H., Wang, Z., Zhang, J., Wang, J. and Shuai, S. (2017). Study on combustion and emission characteristics of polyoxymethylene dimethyl ethers/diesel blends in light-duty and heavy-duty diesel engines. *Applied Energy*, **185**, 1393–1402.

Liu, J., Liu, Z., Wang, L., Wang, P., Sun, P., Ma, H. and Wu, P. (2021). Effects of PODE/diesel blends on particulate matter emission and particle oxidation characteristics of a common-rail diesel engine. *Fuel Processing Technology*, **212**, 106634.

Liu, J., Wang, H., Li, Y., Zheng, Z., Xue, Z., Shang, H. and Yao, M. (2016). Effects of diesel/PODE (polyoxymethylene dimethyl ethers) blends on combustion and emission characteristics in a heavy duty diesel engine. *Fuel*, **177**, 206–216.

Liu, J., Yang, J., Sun, P., Gao, W., Yang, C. and Fang, J. (2019). Compound combustion and pollutant emissions characteristics of a common-rail engine with ethanol homogeneous charge and polyoxymethylene dimethyl ethers injection. *Applied Energy*, **239**, 1154–1162.

Meng, X., Hu, E., Yoo, K. H., Boehman, A. L. and Huang, Z. (2019). Experimental and numerical study on autoignition characteristics of the polyoxymethylene dimethyl ether/diesel blends. *Energy & Fuels* **33**, **3**, 2538–2546.

Mustafi, N. N., Raine, R. R. and James, B. (2010). Characterization of exhaust particulates from a dual fuel engine by TGA, XPS, and Raman techniques. *Aerosol Science and Technology* **44**, **11**, 954–963.

Pan, M., Wu, C., Qian, W., Wang, Y., Huang, H., Zhou, X. and Wei, J. (2022). Impact of dimethoxymethane-diesel fuel blends on the exhaust soot's evolutionary behavior. *Fuel*, **309**, 122221.

Pellegrini, L., Marchionna, M., Patrini, R., Beatrice, C., Del Giacomo, N. and Guido, C. (2012). Combustion behaviour and emission performance of neat and blended polyoxymethylene dimethyl ethers in a light-duty diesel engine. *SAE World Cong. & Exhibition*, Detroit, Michigan, USA.

Pellegrini, L., Marchionna, M., Patrini, R. and Florio, S. (2013). Emission performance of neat and blended polyoxymethylene dimethyl ethers in an old light-duty diesel car. *SAE Paper No*. 2013-01-1035.

Pirjola, L., Rönkkö, T., Saukko, E., Parviainen, H., Malinen, A., Alanen, J. and Saveljeff, H. (2017). Exhaust emissions of non-road mobile machine: Real-world and laboratory studies with diesel and HVO fuels. *Fuel*, **202**, 154–164.

Qu, L. (2017). *Study on the formation and characteristics of particles with biodiesel blend fuels in the exhaust gas atmosphere*. Ph.D. Dissertation. Jiangsu University, Zhenjiang, China.

Ren, S., Wang, Z., Li, B., Liu, H. and Wang, J. (2019). Development of a reduced polyoxymethylene dimethyl ethers (PODEn) mechanism for engine applications. *Fuel*, **238**, 208–224.

Roy, M. M., Calder, J., Wang, W., Mangad, A. and Diniz, F. C. M. (2016). Cold start idle emissions from a modern Tier-4 turbo-charged diesel engine fueled with diesel-biodiesel, diesel-biodiesel-ethanol, and diesel-biodiesel-diethyl ether blends. *Applied Energy*, **180**, 52–65.

Savic, N., Rahman, M. M., Miljevic, B., Saathoff, H., Naumann, K. H., Leisner, T., Riches, J., Gupta, B., Motta, N., and Ristovski, Z. D. (2016). Influence of biodiesel fuel composition on the morphology and microstructure of particles emitted from diesel engines. *Carbon*, **104**, 179–189.

Shah, A. N., Ge, Y., Tan, J., Liu, Z., He, C. and Zeng, T. (2012). Characterization of polycyclic aromatic hydrocarbon emissions from diesel engine retrofitted with selective catalytic reduction and continuously regenerating trap. *J. Environmental Sciences* **24**, **8**, 1449–1456.

Shi, Y., Cai, Y., Li, X., Ji, L., Chen, Y. and Wang, W. (2019). Evolution of diesel particulate physicochemical properties using nonthermal plasma. *Fuel*, **253**, 1292–1299.

Smith, M., Scudiero, L., Espinal, J., McEwen, J. S. and

Garcia-Perez, M. (2016). Improving the deconvolution and interpretation of XPS spectra from chars by ab initio calculations. *Carbon*, **110**, 155–171.

Suhaimi, H., Adam, A., Mrwan, A. G., Abdullah, Z., Othman, M. F., Kamaruzzaman, M. K. and Hagos, F. Y. (2018). Analysis of combustion characteristics, engine performances and emissions of long-chain alcohol-diesel fuel blends. *Fuel*, **220**, 682–691.

Sukjit, E., Herreros, J. M., Dearn, K. D., García-Contreras, R. and Tsolakis, A. (2012). The effect of the addition of individual methyl esters on the combustion and emissions of ethanol and butanol-diesel blends. *Energy* **42**, **1**, 364–374.

Sun, R., Chen, Z. and Li, K. (2013). Proportion optimization of ethanol-diesel fuel and engine performance test. *Trans. Chinese Society of Agricultural Engineering* **29**, **9**, 55–63.

Tan, Y. R., Botero, M. L., Sheng, Y., Dreyer, J. A., Xu, R., Yang, W. and Kraft, M. (2018). Sooting characteristics of polyoxymethylene dimethyl ether blends with diesel in a diffusion flame. *Fuel*, **224**, 499–506.

Tian, J., Cai, Y., Shi, Y., Cui, Y. and Fan, R. (2019). Effect of polyoxymethylene dimethyl ethers/diesel blends on fuel properties and particulate matter oxidation activity of a light-duty diesel engine. *Int. J. Automotive Technology* **20**, **2**, 277–288.

Wang, H. W., Zhou, L. B., Jiang, D. M. and Huang, Z. H. (2000). Study on the performance and emissions of a compression ignition engine fuelled with dimethyl ether. *Proc. Institution of Mechanical Engineers, Part D: J. Automobile Engineering* **214**, **1**, 101–106.

Wang, L., Song, C., Song, J., Lv, G., Pang, H. and Zhang, W. (2013). Aliphatic C–H and oxygenated surface functional groups of diesel in-cylinder soot: Characterizations and impact on soot oxidation behavior. *Proc. Combustion Institute* **34**, **2**, 3099–3106.

Wang, X., Wang, Y., Guo, F., Wang, D. and Bai, Y. (2020). Physicochemical characteristics of particulate matter emitted by diesel blending with various aromatics. *Fuel*, **275**, 117928.

Weng, J. Q., Shen, Y. G., Zhang, X. L. and Fan, Y. L. (2008). The corrosion wear of biodiesel on diesel engine and its mechanism analysis. *Lubrication Engineering* **33**, **8**, 54–57.

Weng, S. (2010). *Fourier Transform Infrared Spectroscopy*. 2nd edn. Chemical Industry Press. Beijing, China.

Xie, M., Ma, Z. J., Wang, Q. H., Liu, J. C. and Liu, S. H. (2017). Investigation of engine combustion and emission performance fuelled with neat PODE and PODE/diesel blend. *J. Xi'an Jiaotong University* **51**, **3**, 32–37.

Yu, Y., Gang, L., Song, C., Song, J., Hao, B., Li, B. and Sun, H. (2016). Impact of oxidation reaction temperature on surface functional groups transformation of diesel particles. *J. Combustion Science and Technology* **22**, **1**, 37–44.

Zhang, P., He, J., Chen, H., Zhao, X. and Geng, L. (2020). Improved combustion and emission characteristics of ethylene glycol/diesel dual-fuel engine by port injection timing and direct injection timing. *Fuel Processing Technology*, **199**, 106289.

Zhang, W. (2009). Effect of dimethyl carbonate on emission characteristics of diesel engines. *Chemical Engineering (China)* **37**, **8**, 59–62.

Zhang, W., Wei, X., Kin, D. and Zhu, Y. (2016). Experimental study on the influence of polyoxymethylene dimethyl ethers (PODE) on ultrafine particle emission of a compression ignition engine. *J. Automotive Safety and Energy* **7**, **3**, 330–336.

Zhang, X., Wu, P., Jiang, Z., Gao, X., Liu, T. and Hu, Y. (2015). Thermodynamic analysis on synthesis of polyoxymethylene dimethyl ethers. *Chemical Engineering (China)* **43**, **4**, 39–44.

Zhao, Y., Xu, Z., Chen, H., Fu, Y. and Shen, J. (2013). Mechanism of chain propagation for the synthesis of polyoxymethylene dimethyl ethers. *J. Energy Chemistry* **22**, **6**, 833–836.w

Zhou, X. (2017). *Study on emission characteristics of particulate matter emitted from diesel engine fueled with blending biodiesel*. M. S. thesis. Jiangsu University. Zhenjiang, China.